AD_____

Award Number: DAMD17-99-1-9456

TITLE: Structure of the Tetrameric p53 Tumor Suppressor Bound to DNA

PRINCIPAL INVESTIGATOR: Ronen Marmorstein, Ph.D.

CONTRACTING ORGANIZATION: The Wistar Institute
Philadelphia, Pennsylvania 19104

REPORT DATE: May 2001

TYPE OF REPORT: Annual

PREPARED FOR: U.S. Army Medical Research and Materiel Command
Fort Detrick, Maryland 21702-5012

DISTRIBUTION STATEMENT: Approved for Public Release;
Distribution Unlimited

REPORT DOCUMENTATION PAGE

Form Approved
OMB No. 074-0188

1. AGENCY USE ONLY (Leave blank)	2. REPORT DATE	3. REPORT TYPE AND DATES COVERED
	May 2001	Annual (15 Apr 00 - 14 Apr 01)

4. TITLE AND SUBTITLE

STRUCTURE OF THE TETRAMERIC P53 TUMOR SUPPRESSOR BOUND TO DNA

5. FUNDING NUMBERS

DAMD17-99-1-9456

6. AUTHOR(S)

Ronen Marmorstein, Ph.D.

7. PERFORMING ORGANIZATION NAME(S) AND ADDRESS(ES)

The Wistar Institute
Philadelphia, Pennsylvania 19104

Marmor@wistar.upenn.edu

8. PERFORMING ORGANIZATION REPORT NUMBER

9. SPONSORING / MONITORING AGENCY NAME(S) AND ADDRESS(ES)

U.S. Army Medical Research and Materiel Command
Fort Detrick, Maryland 21702-5012

10. SPONSORING / MONITORING AGENCY REPORT NUMBER

11. SUPPLEMENTARY NOTES

Report contains color graphics

12a. DISTRIBUTION / AVAILABILITY STATEMENT

Approved for Public Release; Distribution Unlimited

12b. DISTRIBUTION CODE

13. Abstract *(Maximum 200 Words)* *(abstract should contain no proprietary or confidential information)*

The p53 transcriptional activator binds DNA as a tetramer to activate the transcription of genes involved in cell cycle arrest and apoptosis, and alterations in the DNA-binding core domain of p53 are the most common genetic changes found in breast cancer. The overall goal of this proposal is to determine the X-ray crystal structure of a tetrameric form of p53 bound to DNA. Over the last year we determined the structure of the core domain of p53 in the absence of DNA and have described the results of this work in the *Journal of Biological Chemistry*. We have also made progress towards the structure determination of a tetrameric form of p53 bound to DNA. Specifically, we have overexpressed in bacteria two relevant protein constructs of p53 that are competent for tetramer formation on DNA; p53(86-391), and full-length p53. We have purified the p53(86-391) construct to homogeneity and cocrystallization efforts with DNA for structure determination are underway. The structure of tetrameric p53 bound to DNA will provide mechanistic insights into the structural basis underlying p53 mutations, and will provide a framework for the structure-based design of drugs that will be useful in the treatment of p53-mediated breast cancer.

14. SUBJECT TERMS

Breast Cancer, Tetrameric, p53, DNA

15. NUMBER OF PAGES

16

16. PRICE CODE

17. SECURITY CLASSIFICATION OF REPORT	18. SECURITY CLASSIFICATION OF THIS PAGE	19. SECURITY CLASSIFICATION OF ABSTRACT	20. LIMITATION OF ABSTRACT
Unclassified	Unclassified	Unclassified	Unlimited

Table of Contents

(5) INTRODUCTION

The p53 tumor suppressor protein functions as a checkpoint during the G1/S cell cycle transition, responding to DNA damage by activating transcription of genes that encode proteins inducing cell cycle arrest or apoptosis (Burns and El-Deiry, 1999; Prives and Hall, 1999). Alterations in p53 are the most common genetic changes found to date in breast cancer, suggesting that the gene plays a central role in the development of the disease [(Levine, 1997) and http://www.iarc.fr/p53homepage.html]. The transcriptional activity of p53 is mediated by a tetrameric form of the protein that binds DNA in a sequence-specific fashion to activate the transcription of target genes (El-Deiry et al., 1993; Friedman et al., 1993; Halazonetis and Kandil, 1993; Stenger et al., 1994). p53 contains four functionally distinct domains: a loosely folded N-terminal transcriptional activation domain (residues 1 to 44), a central core (residues 102 to 292) containing a DNA binding domain, a tetramerization region (residues 320 to 356), and a regulatory domain (residues 356-393) (Cho et al., 1994; Pavletich et al., 1993; Wang et al., 1993). The vast majority of tumor-derived p53 mutations are localized to the core domain and thus prevent p53 from binding DNA (Cho et al., 1994). The overall goal of this proposal is to understand the structural basis for the inability of tumor-derivedp53 mutants to bind DNA by determining the X-ray crystal structure of tetrameric forms of p53 bound to DNA.

The specific technical objectives of this proposal are to (1) Prepare p53 protein and DNA target sites for p53/DNA cocrystallization (tasks 1-4), (2) Crystallize the p53/DNA complex for structure determination using X-ray crystallography (tasks 5 and 6), (3) Determine the three-dimensional structure of a p53/DNA complex (tasks 7-13), and (4) Overexpress and purify to homogeneity the p53-T284R mutant protein that is able to rescue common tumor-derived p53-mutations, crystallize it bound to DNA, and determine the structure of the p53-T284R/DNA complex (tasks 14-20). The structure of the p53/DNA complex will provide a mechanistic understanding into the structural basis for how p53 mutations result in mammary carcinomas, and a comparison with the p53-T284R/DNA structure will provide a framework for the structure-based design of drugs that may mimic the T284R mutation (Wieczorek et al., 1996) and thus will be useful in the treatment of p53-mediated breast cancer.

(6) BODY

During the first year of the funding period we accomplished the following: (1) we cloned, overexpressed and purified to homogeneity two relevant protein constructs of mouse p53 that are competent for tetramer formation on DNA; p53(98-292) harboring the p53 core domain, and p53(86-351) harboring the core-linker-tetramirization region of p53 (technical objective 1, tasks 1), and (2) and characterized the biophysical and DNA properties of these proteins (technical objective 1, tasks 2-4). In addition, we had prepared well diffracting crystals of an apparent p53(98-292)/DNA complex (Technical objective 2,tasks 5 and 6).

During the second year of the funding period we completed the structure determination of the apparent p53(98-292)/DNA complex. Surprisingly, we found that the crystals contained

protein, but not DNA. Thus the structure yielded the first image of the p53 core domain in the absence of DNA. The results of this work are described in a publication in the *Journal of Biological Chemistry* and is included in the appendix of this report. In summary we found that like the human p53 core domain in complex with DNA, the p53 core domain in the absence of DNA adopted an immunoglobulin-like β sandwich architecture with a series of loops and short helices at opposite ends of the β sandwich. Comparison of the DNA-bound and DNA-free p53 core domains revealed that while the central β sandwich architecture remains largely unchanged, a loop region important for DNA binding undergoes significant rearrangement. While this loop region mediates major groove DNA contacts in the DNA-bound structure, it adopts a conformation that is incompatible with DNA-binding in the DNA-free structure. Interestingly, crystals of the DNA-free core domain contain a non-crystallographic trimer with three nearly identical subunit-subunit (dimer) contacts. These dimer contacts align the p53 core domains in a way that is incompatible with simultaneous DNA-binding by both protomers of the dimer. Surprisingly, similar dimer contacts are observed in crystals of the human p53 core domain with DNA in which only one of the three p53 protomers in the asymmetric unit cell are specifically bound to DNA. Based on these findings, we propose that the p53 core domain dimer that is seen in the crystals of the free core domain represents a physiologically relevant inactive form of p53 that must undergo structural rearrangement for sequence-specific DNA binding.

Although we have obtained interesting results from the structure of the p53 core domain in the absence of DNA and these results have implications for how p53 binds DNA, thus far attempts to obtain crystals that contain a tetrameric form of p53 bound to DNA have not been successful (technical objective 2). In addition to our inability to cocrystallize the p53 core domain with DNA, we have been unable to crystallize the p53(86-351) domain construct bound to DNA. In order to increase our chances of obtaining cocrystals we have recently prepared two other recombinant forms of p53, p53 (86-391) (containing the core domain, linker, tetramerization domain and the DNA regulatory domain), and p53 full length (residues 3-391, also containing the N-terminal transactivation domain). Both protein constructs overexpress to high levels in bacteria and are found in the soluble protein fraction. We have recently purified the p53(86-391) construct to homogeneity (Figure 1) and crystallization trials with DNA are underway (technical objective 2, task 5).

(7) KEY RESEARCH ACCOMPLISHMENTS

- Structure determination and publication of the mouse p53 core domain [p53(98-292)].
- Overexpression and purification to homogeneity of a mouse p53 (86-391) protein construct harboring the core domain, linker region, teramerization domain and DNA regulatory region.
- Crystallization efforts of mouse p53 (86-391) with DNA.
- Overexpression of a full-length mouse p53 protein construct [p53(3-391)].

(8) REPORTABLE OUTCOMES

Zhao, K., Chai, X., Johnston, K., Clements, A. and Marmorstein, R. "Crystal structure of the mouse p53 core DNA-binding domain at 2.7Å resolution," (2001) *J. Biol. Chem.*, 276, 12120-12127.

(9) CONCLUSIONS

During the first year of the proposal we had prepared two mouse p53 protein constructs, one harboring the isolated core domain [p53(98-292)] and the other harboring the core domain, linker and tetramerization domain [p53(86-351)]. Although we were unable to cocrystallize these protein constructs with DNA, the core domain construct yielded crystals in the absence of DNA.

During the second year of the funding period we completed the structure determination of the p53 core domain in the absence of DNA and a comparison with the previously determined core p53 domain in the presence of DNA revealed important details about how p53 undergoes structural rearrangement for DNA binding. To further pursue the structure of a tetrameric form of p53 in complex with DNA we have prepared two additional p53 protein constructs p53(86-391), and full-length p53 (residues 3-391). Both proteins have been overexpressed in bacteria and the p53(86-391) construct has been purified to homogeneity and crystallization trails with DNA are underway (through task 5 of technical objective 2).

During the third year of the grant period we expect to obtain crystals of either the p53(86-351) or p53 full length protein constructs bound as tetramers to DNA (technical objective 2), and use these crystals to determine the structure of the protein/DNA complex (technical objective 3). This structure will set the stage for the completion of the final technical objective of the proposal (technical objective 4). The final objective of the proposal is to determine the structure of the DNA complex with the T284R p53 mutant protein that rescues tumor derived mutations. A comparison of this structure with the native structures is expected to provide a framework for the structure-based design of drugs that may mimic the T284R mutation and thus will be useful in the treatment of p53-mediated breast cancer.

(10) REFERENCES

Burns, T. F., and El-Deiry, W. S. (1999). The p53 pathway and apoptosis. J. Cell Physiol. *181*, 231-239.

Cho, Y., Gorina, S., Jeffrey, P. D., and Pavletich, N. P. (1994). Crystal structure of a p53 tumor suppressor-DNA complex: understanding tumorigenic mutations. Science *265*, 346-355.

El-Deiry, W. S., Tokino, T., Velculescu, V. E., Levy, D. B., Parsons, R., Trent, J. M., Lin, D., Mercer, W. E., Kinzler, K. W., and Vogelstein, B. (1993). WAF1, a potential mediator of p53 tumor suppression. Cell, 817-825.

Friedman, P. N., Chen, X. B., Bargonetti, J., and Prives, C. (1993). The p53 protein is an unusually shaped tetramer that binds directly to DNA. Proc. Natl. Acad. Sci. U. S. A. *90*, 5878-5878.

Halazonetis, T. D., and Kandil, A. N. (1993). Conformational shifts propagate from the oligomerization domain of p53 to its tetrameric DNA-binding domain and restore DNA- binding to select p53 mutants. Embo J. *12*, 5057-5064.

Levine, A. J. (1997). p53, the cellular gatekeeper for growth and division. Cell *88*, 323-331.

Pavletich, N. P., Chambers, K. A., and Pabo, C. O. (1993). The DNA binding domain of p53 contains the four conserved regions and the four major mutation hot spots. Genes & Develop. *7*, 2556-2564.

Prives, C., and Hall, P. (1999). The p53 pathway. J. Pathol. *187*, 112-126.

Stenger, J. E., Tegtmeyer, P., Mayr, G. A., Reed, M., Wang, Y., Wang, P., Hough, P. V. C., and Mastrangelo, I. A. (1994). p53 oligomerization and DNA looping are linked with transcriptional activation. Embo J. *13*, 6011-6020.

Wang, Y., Reed, M., Wang, P., Stenger, J. E., Mayr, G., Anderson, M. E., Swhwedes, J. F., and Tegtmeyer, P. (1993). p53 domains: identification and characterization of two autonomous DNA-binding domains. Genes & Dev. *7*, 2575-2586.

Wieczorek, A. M., Waterman, J. L. F., Waterman, M. J. F., and Halazonetis, T. D. (1996). Structure-based rescue of common tumor-derived p53 mutants. Nature Medicine *2*, 1143-1146.

(11) APPENDICES

Figure 1

Zhao, K., Chai, X., Johnston, K., Clements, A. and Marmorstein, R. "Crystal structure of the mouse p53 core DNA-binding domain at 2.7Å resolution," (2001) *J. Biol. Chem.*, 276, 12120-12127.

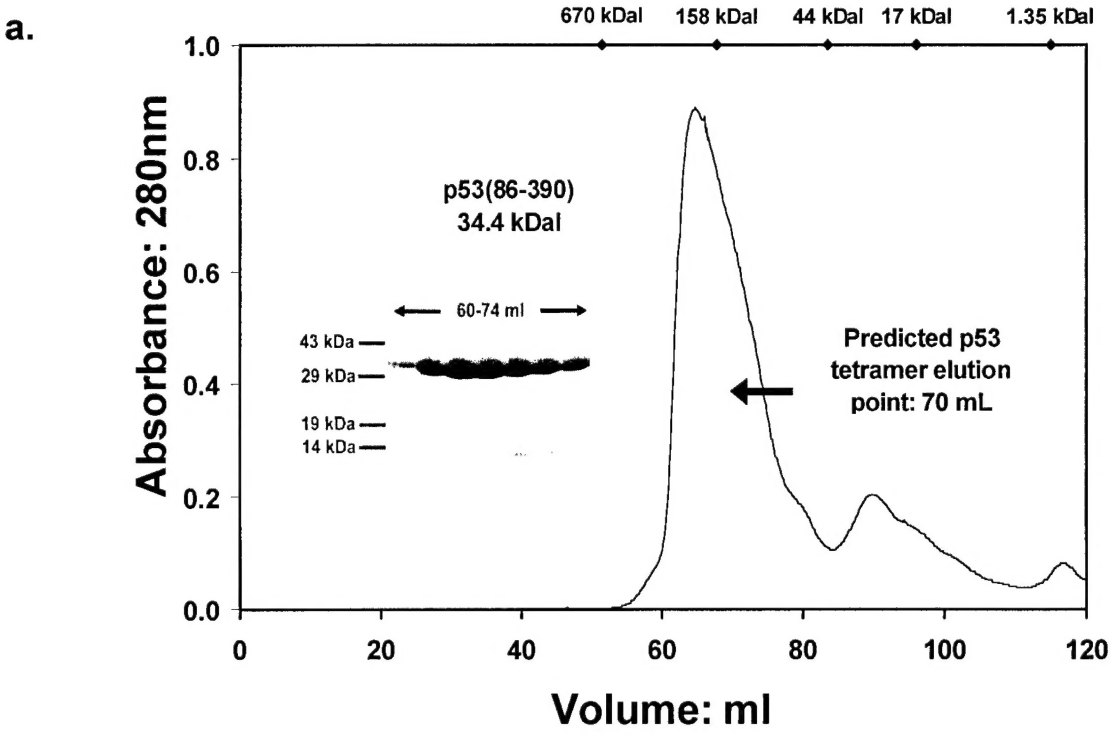

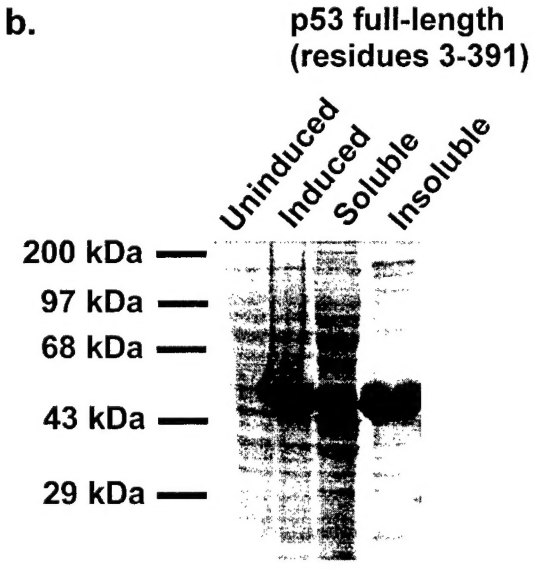

Figure 1. Preparation of the mouse p53(86-391) and p53 full-length (residues 3-391) protein constructs. (a) Purification of p53(86-391). The protein was purified using a combination of cation exchange and gel filtration chromatography. The final gel filtration chromatograph on a Superdex-200 gel-filtration FPLC column is shown with the corresponding peak fractions illustrated on the embedded SDS-PAGE gel. (b) Overexpression of p53 full-length. An SDS-PAGE gel is shown for uninduced, IPTG-induced, soluble and insoluble protein fraction (lane4). The gel illustrates that a significant fraction of the p53 full-length protein construct is in the soluble protein fraction and is therefore amenable to purification for cocrystallization efforts with DNA.

THE JOURNAL OF BIOLOGICAL CHEMISTRY
Vol. 276, No. 15, Issue of April 13, pp. 12120–12127, 2001
Printed in U.S.A.

Crystal Structure of the Mouse p53 Core DNA-binding Domain at 2.7 Å Resolution*

Received for publication, December 22, 2000
Published, JBC Papers in Press, January 4, 2001, DOI 10.1074/jbc.M011644200

Kehao Zhao‡, Xiaomei Chai‡, Karen Johnston‡, Adrienne Clements‡§, and Ronen Marmorstein‡§¶‖

From the ‡The Wistar Institute and the ¶Department of Chemistry, University of Pennsylvania and the §Department of Biochemistry and Biophysics, University of Pennsylvania School of Medicine, Philidelphia, Pennsylvania 19104

The p53 tumor suppressor is a sequence-specific DNA-binding protein that activates transcription in response to DNA damage to promote cell cycle arrest or apoptosis. The p53 protein functions in a tetrameric form *in vivo* and contains four domains including an N-terminal transcriptional activation domain, a C-terminal regulatory domain, a tetramerization domain, and a central core DNA-binding domain that is the site of the majority of tumor-derived mutations. Here we report the 2.7-Å crystal structure of the mouse p53 core domain. Like the human p53 core domain in complex with DNA, the mouse p53 core domain adopts an immunoglobulin-like β sandwich architecture with a series of loops and short helices at opposite ends of the β sandwich. Comparison of the DNA-bound and DNA-free p53 core domains reveals that while the central β sandwich architecture remains largely unchanged, a loop region important for DNA binding undergoes significant rearrangement. Although this loop region mediates major groove DNA contacts in the DNA-bound structure, it adopts a conformation that is incompatible with DNA binding in the DNA-free structure. Interestingly, crystals of the DNA-free core domain contain a noncrystallographic trimer with three nearly identical subunit-subunit (dimer) contacts. These dimer contacts align the p53 core domains in a way that is incompatible with simultaneous DNA binding by both protomers of the dimer. Surprisingly, similar dimer contacts are observed in crystals of the human p53 core domain with DNA in which only one of the three p53 protomers in the asymmetric unit cell is specifically bound to DNA. We propose that the p53 core domain dimer that is seen in the crystals described here represents a physiologically relevant inactive form of p53 that must undergo structural rearrangement for sequence-specific DNA binding.

The p53 tumor suppressor protein functions as a checkpoint during the G_1/S cell cycle transition, responding to DNA damage by activating transcription of genes that encode proteins inducing cell cycle arrest or apoptosis (1, 2). Disruption of the G_1/S cell cycle transition and mutation of the p53 protein in particular occur in a variety of cancer types and correlate with the majority of human cancers (3).[1] The majority of p53 tumor-derived mutations are now known to inactivate its DNA binding properties and therefore to impair its ability to activate transcription (4).

The transcriptional activity of p53 is mediated by a tetrameric form of the protein that binds DNA in a sequence-specific fashion to activate the transcription of target genes (5–8). Each p53 subunit contains four functionally distinct domains: a loosely folded N-terminal transcriptional activation domain (residues 1–44), a central core (residues 102–292) containing a DNA-binding domain, a tetramerization region (residues 320–356), and a regulatory domain (residues 356–393) (4, 9, 10). There are over 100 naturally occurring p53 DNA target sequences, and the human genome has been estimated to contain about 200–300 of such sites (11). Although the sequences of these p53 DNA target sites show variability, they all contain two head to tail decamers each containing a pentameric inverted repeat. Most decamers contain the consensus sequence PuPuPuC(A/t) ↓ (T/a)GPyPyPy, where Pu and Py are purines and pyrimidines, respectively (12). Although the various domains of the p53 protein can function autonomously, *in vivo* activity requires the intact protein. In addition, various lines of evidence suggest that the intact protein exists in two conformational states, one that has low affinity for DNA (T state) and another that has a high affinity for DNA (R state) (6, 13).

Significant insights into the tetramerization and DNA binding properties of p53 are revealed by the structures of the isolated tetramerization domain (14–16) and of the human p53 core domain bound as a monomer to DNA (4), respectively. The structure of the tetramerization domain reveals a dimer of dimers. The structure of the p53 core domain bound to DNA reveals the details of monomer binding to a pentameric DNA sequence. These findings were used to rationalize the functional consequence of the majority of tumor-derived p53 mutations by showing that they map to regions of the core domain that would either affect the stability of the core domain itself or destabilize protein-DNA contacts. Despite the insights that are gained from the structural analysis of p53, several questions underlying p53 structure/function still remain. Among these questions is the issue of the nature of the structural rearrangements that p53 undergoes upon DNA binding.

We report here the crystal structure of the mouse p53 core domain in the absence of DNA. A comparison with the crystal structure of the human p53 core domain bound as a monomer to DNA reveals that the overall structure of the core domain remains largely unperturbed upon DNA binding except for a

* This work was supported by Grant DAMD17-99-1-9456 from the United States Army Breast Cancer Research Program (to R. M.). The costs of publication of this article were defrayed in part by the payment of page charges. This article must therefore be hereby marked "*advertisement*" in accordance with 18 U.S.C. Section 1734 solely to indicate this fact.

The atomic coordinates and structure factors (code 1HU8) have been deposited in the Protein Data Bank, Research Collaboratory for Structural Bioinformatics, Rutgers University, New Brunswick, NJ (http://www.rcsb.org/).

‖ To whom correspondence should be addressed: The Wistar Inst., 3601 Spruce St., Philadelphia, PA 19104. Tel: 215-898-5006; Fax: 215-898-0381; E-mail: marmor@wistar.upenn.edu.

[1] Contact the corresponding author for an additional Web address.

pronounced movement of a loop region. This loop region adopts a conformation that is incompatible with DNA binding in the DNA-free structure but adopts a conformation that facilitates major groove DNA contacts in the DNA-bound structure. Moreover, the crystals analyzed here, reveal a noncrystallographic trimer with three nearly identical subunit-subunit (dimer) contacts. These dimer contacts align the p53 core domains in a way that is incompatible with simultaneous DNA binding by both protomers of the dimer. Interestingly, similar dimer contacts are observed in crystals of the human p53 core domain with DNA in which only one of three p53 protomers in the asymmetric unit cell is specifically bound to DNA. We discuss the implications of these findings for DNA-induced structural rearrangements of the p53 core domain in the context of the intact p53 tetramer.

TABLE I
Data collection and refinement statistics

Space group	$C222_1$
Cell dimensions (Å)	a = 73.68
	b = 119.99
	c = 184.24
Resolution (Å)	10–2.7
No. of observations	121009
No. of unique reflections	22733
Completeness/last shell	99.5/98.7%
Multiplicity	5.3
I/σ(I)/last shell	9.6/3.9
R-merge[a]/last shell	0.051/0.189
No. of reflections ($F > 2\sigma(F)$)	22252
No. of protein atoms	4381
No. of zinc atoms	3
No. of water atoms	108
R-factor[b]	23.9
R-free[c]	29.9
Mean B value (Å)	67.2
r.m.s.d. bonds (Å)[d]	0.007
r.m.s.d. angles (°)	1.32
Dihedral angles (°)	25.0
Improper angles (°)	0.89

[a] R-merge = $\Sigma_h\Sigma_i|I_{h,i} - I_h|/\Sigma_h\Sigma I_{h,i}$ where I_h is the mean intensity of symmetry-related reflections, $I_{h,i}$.

[b] R-factor = $\Sigma||F_o| - |F_c||/\Sigma|F_o|$ where F_o and F_c are the observed and calculated structure factor amplitudes, respectively.

[c] R-free is calculated for the 10% of the data that was withheld from refinement.

[d] r.m.s.d., root mean square deviation.

MATERIALS AND METHODS

Purification and Crystallization of the Mouse p53 Core Domain—The DNA sequence encoding the mouse p53 core domain (residues 92–292) was amplified from the plasmid p11-4 (obtained from A. Levine, Princeton University) by polymerase chain reaction and subcloned into the pRSET (Invitrogen) bacterial expression vector. The plasmid was transformed into the *Escherichia coli* BL21/DE-3 strain. Cells were initially grown in LB medium at 37 °C. When cultures reached an absorbance at 595 nm of ~0.4–0.6, cells were induced by the addition of 0.5 mM isopropyl-1-thio-β-D-galactopyranoside (supplemented with 100 μM zinc acetate) and grown overnight at 15 °C. The cells were isolated by centrifugation and resuspended in low salt buffer A (20 mM sodium citrate, pH 6.1, 100 mM NaCl, 10 μM Zn^{2+}, and 10 mM dithiothreitol). The cells were sonicated, and cellular debris was removed by centrifugation. The supernatant containing soluble mouse p53 core domain was loaded onto a SP-Sepharose (Amersham Pharmacia Biotech) ion exchange column, which was washed with 20× column volumes of buffer A, and the protein was eluted with a 0.1–1.0 M NaCl gradient. Peak fractions containing p53 core domain were pooled and concentrated using a Centriprep-10 (Amicon) and further purified by gel filtration chromatography using a Superdex-75 column. Peak fractions were judged to be greater than 97% homogeneous by SDS-polyacrylamide gel electrophoresis analysis, concentrated to ~40–55 mg/ml, and stored at −80 °C until further use.

Crystallization attempts were initially directed at obtaining a complex of the p53 core domain bound as a tetramer to a 24-base-paired DNA duplex containing four pentameric DNA binding sites. To this end, 10 mg/ml protein was mixed with a 0.25 molar equivalent of DNA duplex and screened for crystallization against a crystallization screen

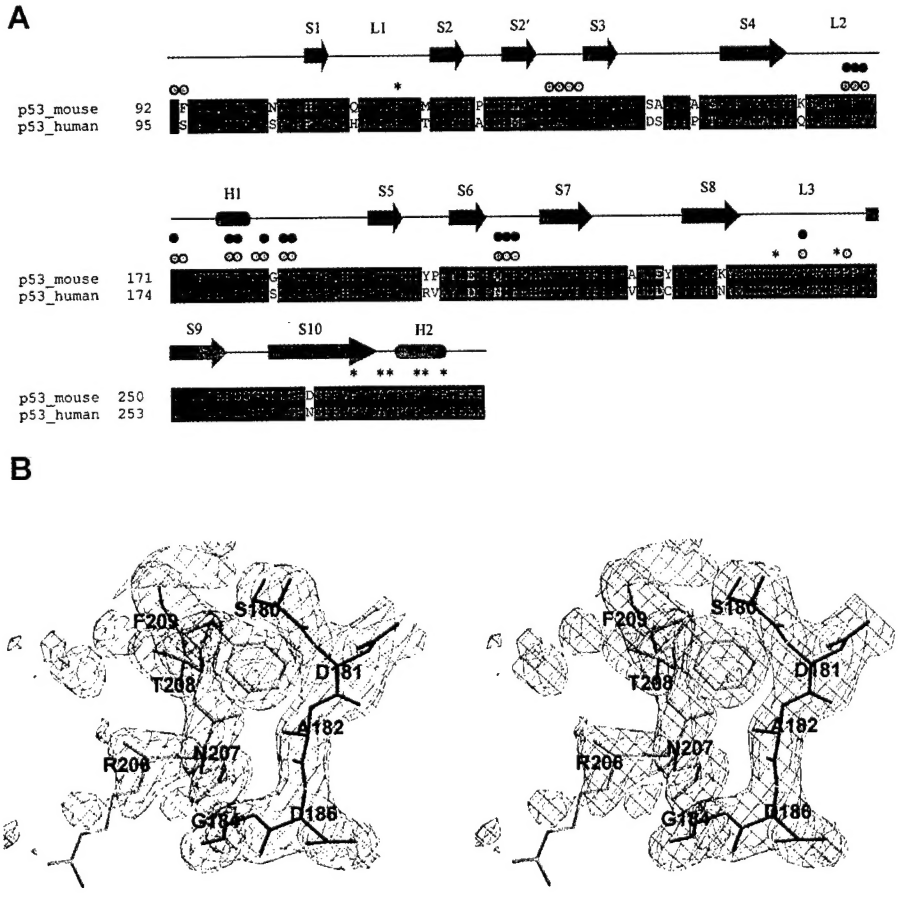

FIG. 1. *A*, sequence alignment of the p53 core domains from mouse and human. Sequences are aligned using the CLUSTAL program and displayed with the BOXSHADE program. *Black* and *gray backgrounds* are used to indicate identical and conserved residues at a given position, respectively. Secondary structural elements within the mouse p53 core domain are shown above the sequence alignment. The *circle* symbols indicate residues that are associated with the dimer interface of the mouse DNA-free (*black circle*) and human DNA-bound (*gray circle*) p53 core domain, and the * symbol indicates residues of the human p53 core domain that contact DNA in the human p53 core-DNA complex. *B*, representative $F_o - F_c$ omit electron density map of the refined mouse p53 core domain structure proximal to the dimer interface. The map is contoured at 2.5 σ. The *green* and *red* colors indicate molecules A and B of the p53 core domain within the asymmetric unit cell.

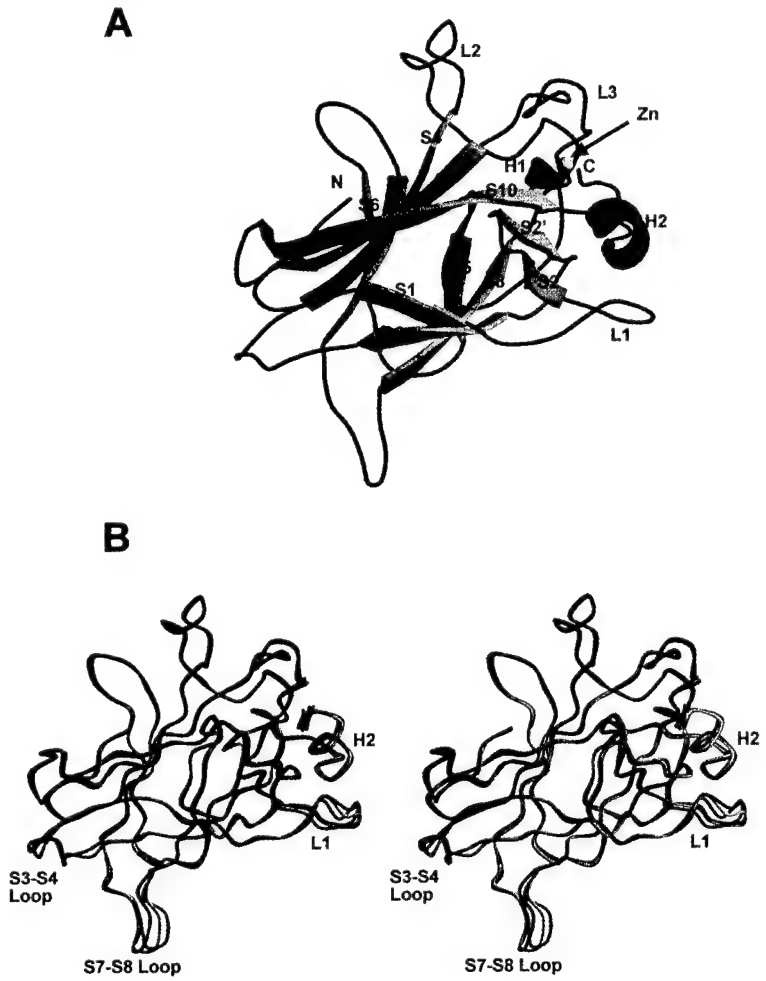

FIG. 2. **Overall structure of the mouse p53 core domain.** *A*, schematic ribbon diagram of the p53 core domain. *B*, Cα superposition of the three p53 protomers in the asymmetric unit cell of the crystals.

for protein-DNA complexes using the hanging drop method. The best crystals were obtained against a reservoir containing 8% polyethylene glycol 4000, 200 mM KCl, 50 mM $MgCl_2$, 10 mM dithiothreitol, and 50 mM Tris-HCl, pH 7.5, and grew to a typical size of 0.2 × 0.4 × 0.4 mm. Subsequent washing of large well formed crystals followed by crystal dissolution and analysis on SDS-polyacrylamide gel electrophoresis and silver staining revealed that these crystals contained the p53 core domain but no DNA.

Data Collection, Structure Determination, and Refinement—Crystals of the mouse p53 core domain were flash-frozen in a cryoprotectant containing the reservoir solution supplemented with 25% polyethylene glycol 400, and diffraction data were collected at 120 K at the A1 station of Cornell High Energy Synchrotron Source using a charged coupled device detector. Data were processed and scaled with MOLSFLM (17). Crystals belong to the orthorhombic space group $C222_1$ with three molecules in the asymmetric unit. The structure was solved by molecular replacement with the program AMoRe (18) using diffraction data from 10 to 3.0 Å. The search model used in the calculation was molecule B of the human p53 core domain (accession number 1TSR). For the search model, residues that differed between the human and mouse p53 core domains were changed to alanine (except for residues 183 and prolines that were changed to glycines). Rotation and translation searches followed by rigid body refinement yielded an unambiguous solution for the three protomers in the asymmetric unit cell with an *R*-factor of 47.5% and a correlation value of 42.4%.

The model was manually rebuilt against $2F_o - F_c$, $F_o - F_c$, and $F_c - F_o$ maps using the program O (19). Rigid body refinement, least square minimization, and simulated annealing refinement with crystallography and NMR suite (20) using noncrystallographic symmetry restraints between the three protomers in the asymmetric unit cell were carried out at a resolution range of 10–3.0 Å. When the data were extended to a 2.7-Å resolution, noncrystallographic symmetry restraints were gradually released, and several cycles of simulated annealing (21), torsion angle dynamic (22), temperature factor refinement, and manual model building were carried out. During the final stages of refinement, a bulk solvent correction was applied to the data (23), water molecules were included using the waterpick routine of crystallography and NMR suite, and three zinc ions were added. Some residues at the very N and C termini were not visible in the electron density map and were therefore not modeled. The final structure contained residues 99–284 of each protomer, had excellent stereochemistry, and had crystallographic *R*-factors of 23.9 and 29.9% for *R*-working and *R*-free, respectively, against data from 10 to 2.7 Å (see Table I and Fig. 1*B*).

Sedimentation Equilibrium Ultracentrifugation—For sedimentation equilibrium experiments, each cell was assembled with a double sector 12-mm centerpiece with sapphire windows. Blank scans with distilled water were taken before interference optics sedimentation equilibrium experiments at appropriate speeds to correct for window distortion of the fringe displacement data (24). Cells were loaded with the mouse p53 core at two different starting concentrations (0.5 and 1.5 mg/ml) in a buffer containing 100 mM NaCl, 10 mM dithiothreitol, and 20 mM Tris-HCl, pH 7.5. The experiment was performed at three separate centrifugation speeds of 22,900, 32,400, and 37,500 rpm. At each speed, fringe displacement scans were collected every 4 h until the protein samples reached equilibrium. Equilibrium was assessed by comparison of successive scans using the MATCH program, and data editing was performed using the REEDIT program (both programs were provided by National Analytical Ultracentrifugation Facility, Storrs, CT).

After equilibrium was obtained, the NONLIN program (25) was used to globally fit the final scans from the two different concentrations and all speeds (a total of six curves were analyzed simultaneously). NONLIN fits used an effective reduced molecular weight, $\sigma = M(1 - \bar{v}\rho)\omega^2/RT$, in which M is the molecular weight, $\bar{v}$ is the partial specific volume, ρ is the solvent density, ω is the angular velocity (2π(rpm)/60), R is the gas constant, and T is the temperature in Kelvin. The partial specific volume of the mouse p53 core was calculated from the amino acid sequence, and the density of the solvent was calculated as described previously (26). For this model of weak self-association, σ was held at the correct value based on the known monomer molecular weight of the protein, and separate equilibrium constants for each scan were fitted as ln K. These values were converted to dissociation constants with the appropriate molar units. The fit quality for the model

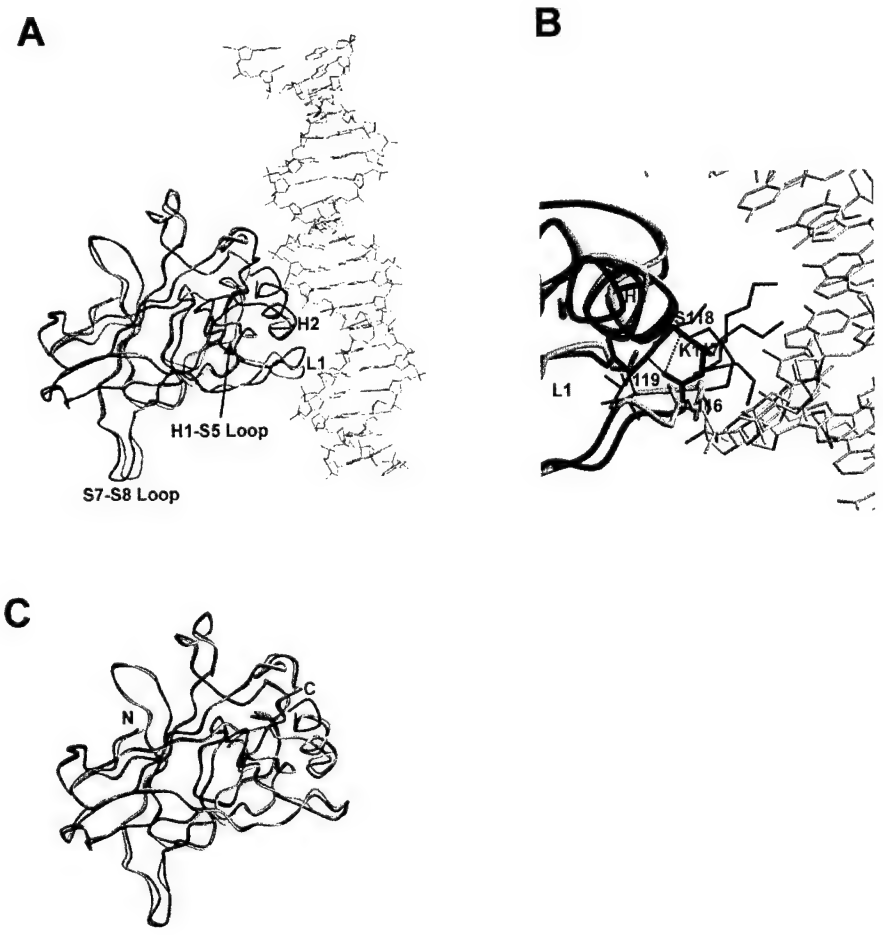

FIG. 3. **Comparison of the DNA-free form of the mouse p53 core domain with the DNA-bound and DNA-free forms of the human p53 core domain.** The DNA-free mouse p53 core domain is shown in *green*, and the human p53 core domain is shown in *red*. *A*, Cα superimposition of the DNA-free mouse p53 core domain with the DNA-bound form of the human p53 core domain. The DNA that is bound to the human p53 core domain is shown in *blue*. *B*, close-up view of the p53-DNA interface proximal to the L1 loop (*A*). The DNA-bound form of the human p53 core domain is shown in *red*, highlighting residues 116–119 of the L1 loop (mouse p53 numbering). The corresponding region of molecule A of the DNA-free mouse p53 core domain is shown in *gray*. The conformations of the Lys-117 side chain in the three mouse p53 core domains in the asymmetric unit cell are shown in *dark gray*. *C*, Cα superimposition of the DNA-free mouse p53 core domain with the DNA-free form of the human p53 core domain.

was determined by examination of residuals and by minimization of the fit variance. The root mean square deviation of the residuals for the multiple species model was 9.56×10^{-3}.

RESULTS AND DISCUSSION

Overall Structure of the p53 Core Domain—The crystal structure presented here contains three molecules of the mouse p53 core domain in the asymmetric unit cell. The overall fold of the p53 core domain is very similar to that of the previously reported core domain in complex with DNA (4) (Figs. 1*A* and 2*A*). Briefly, the core domain forms a central region that adopts an immunoglobulin-like β sandwich architecture of two long twisted antiparallel β sheets of four (S1, S3, S8, and S5) and five (S10, S9, S4, S7, and S6) strands (Figs. 1*A* and 2*A*). Located at opposite ends of the β sandwich are a series of loops. One of the two ends also contains two short helices (H1 and H2) and a tightly bound zinc atom that is tetrahedrally ligated by Cys-173 and His-176 from the L2 loop (between strands S4 and S5) and Cys-235 and Cys-239 from the L3 loop (between strands S8 and S9). The structure of the human p53 core domain bound to DNA shows that the H2 helix, the L3 loop, and the L1 loop (between strands S1 and S2) interact with DNA.

A superposition of the three molecules in the asymmetric unit (Fig. 2*B*) gives root mean square deviation values of 0.40 Å (molecule A-molecule B), 0.57 Å (molecule C-molecule A), and 0.62 Å (molecule B-molecule C) for all main chain atoms. Structural deviations are largely restricted to the L1 loop (residues 115–121) along the DNA-binding side of the core domain and the loops between strands S3 and S4 (residues 220–223) and S7 and S8 (residues 149–151) opposite to the DNA-binding side of the molecule. Although the structural variability within the S3-S4 and S7-S8 loops appears to reflect inherent flexibility within this region of the core domain, as will be discussed below, the structural variability within the L1 loop appears to be due in part to the absence of bound DNA.

Comparison with the Human p53 Core Domain in Complex with DNA—The core domains of human and mouse p53 are highly homologous in sequence with an overall identity of 89%. Therefore a comparison between the nascent mouse p53 core domain and the DNA-bound human p53 core domain can be used to examine the effect of core domain structure as a function of DNA binding. An overall comparison of the nascent (using monomer A) and the DNA-bound form of p53 shows a root mean square deviation between main chain atoms of 0.87 Å as compared with a value between 0.4 and 0.62 Å between noncrystallographically related subunits of the nascent structure (Fig. 3*A*). The larger structural differences that are observed when comparing the unbound and DNA-bound forms of p53 within two different crystal forms are consistent with a comparison between the p53 core domain in the absence of DNA with the DNA-free p53 subunit within the crystal lattice of the p53-DNA complex (Fig. 3*C*). This comparison shows a root mean square deviation between main chain atoms of 0.57 Å. Taken together, DNA binding by the p53 core domain appears to illicit small yet significant structural changes.

The structural changes between the DNA-bound and DNA-free core domains are primarily localized to four regions (Fig. 3*A*). Near the DNA-binding surface structural differences are seen in the L1 loop and the C-terminal end of the H2 helix. Away from the DNA-binding surface structural differences are seen in the loop separating the S7 and S8 strands and the loop between the H1 helix and the S5 strand. Structural differences within the S7-S8 and H1-S5 loops appear to be a function of interactions between the p53 core domains in the crystals, as will be discussed below, whereas structural differences within

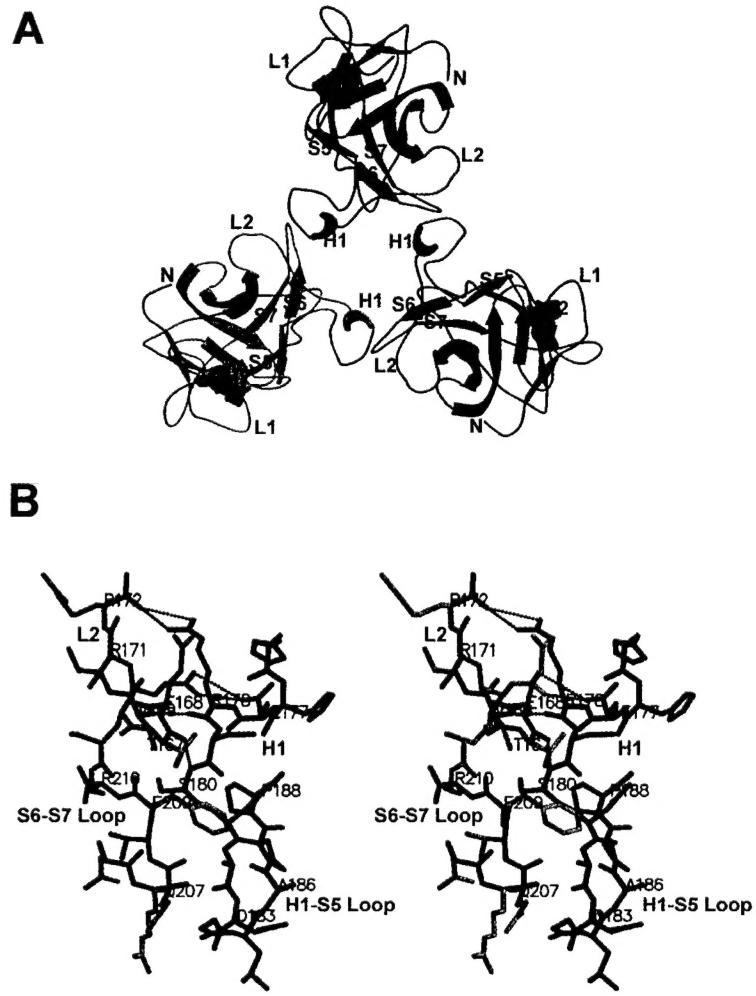

FIG. 4. **Structure of the mouse p53 core domain dimer.** *A*, trimeric packing of the mouse p53 core domain in the asymmetric unit cell viewed perpendicular to the 3-fold axis of the trimer. *B*, stereo diagram showing the intermolecular interaction at the dimer interface of the trimeric structure. Protomer A is shown in *green*, and protomer B is shown in *blue*. *C*, superposition of the mouse p53 core domain dimer (using protomers A and B) with the p53 core domain dimer in crystals of the human core domain in which only one of the two protomers is specifically bound to DNA. The *left view* shows an overall superposition of the dimers, and the *right view* shows a superposition of only one of the protomers of the dimer. This type of superposition shows that the second protomers of the respective dimers are related by a 12 ° rotation. *D*, dimer contacts within the crystals of the human p53 core domain in which only one of the two protomers is specifically bound to DNA.

the L1 loop appear to be a function of DNA binding.

The L1 loop in the DNA-free form of the p53 core is further away from the H2 helix than it is in the DNA-bound form. In fact, a superposition of the DNA-free p53 core onto the core domain of the DNA complex suggests that the L1 loop would clash with the DNA and therefore suggests that the L1 loop would need to move closer to the H2 helix (as it is in the DNA-bound structure) to fit into the major groove of the DNA. Two interactions within the L1 loop appear to stabilize its DNA-bound form over the DNA-free form. Within the L1 loop, Lys-117 (Lys-120 in human p53) is disordered in all three core domains of the asymmetric unit cell (Fig. 3*B*). In contrast, the DNA complex shows that Lys-120 makes contacts to the major groove of the DNA. The conformation of the L1 loop in the DNA bound form is also stabilized by a backbone H bond at the turn of the L1 loop between Ala-116 and Ser-118 (mouse p53 numbering), an interaction that is lost in the DNA-free form (Fig. 3*B*). Taken together, the L1 loop region of the p53 core appears to undergo important structural rearrangement for DNA binding.

Dimer Contacts between p53 Core Domains in the Crystals—The most surprising finding from our crystal structure is that the mouse p53 core domain is packed in the crystals as a noncrystallographic trimer in which the subunits are held together by nearly identical dimer contacts. These dimer contacts are quite extensive and bury a total of ~1458 Å^2 at each interface, which amounts to ~15% of the surface area of each protein subunit (Fig. 4*A*). These dimer contacts involve the H1-S5 loop of one subunit and the S4-H1 (L2) and S6-S7 loops of the other dimer subunit (Fig. 4*B*). The interface is stabilized by both hydrogen bonds and Van der Waals interactions. Main chain hydrogen bonds are formed between residues 168 and 169 of the S4-H1 loop with residues 180 and 178 of the H1-S5 loop of the opposing subunit, respectively, and between residue 207 of the S6-S7 loop with residue 182 of the H1-S5 loop. Side chain hydrogen bonds are also formed in the dimer, and Arg-178 of the H1-S5 loop plays a particularly important role in this regard. The side chain of Arg-178 makes a direct hydrogen bond to the backbone OH of residue 172 of the S4-H1 loop of the opposing subunit and also makes water-mediated interactions to the side chains of Glu-168 and Tyr-160 of the same loop. Van der Waals interactions at the dimer interface involve interactions between Phe-209 of the S6-S7 loop with Ala-182 and Pro-188 of the H1-S5 loop and between Val-169 of the S4-H1 loop with the aliphatic regions of Arg-178 and Ser-180 of the H1-S5 loop.

The dimer interaction in the crystals position the protein segments involved in DNA interaction, the H2 helix and the L1 loop, in a configuration that is incompatible with the simultaneous binding to duplex DNA by both protomers of the dimer. Therefore the dimer in the crystals represents a configuration that is inactive for DNA binding in which each core domain binds a pentameric DNA sequence. The observation that the noncrystallographic trimer mediates identical dimer contacts indicates that the crystallographically observed dimer interface represents a stable minimum. Interestingly, very similar dimer contacts are observed in crystals of the human p53 core domain in the presence of DNA. In these crystals, an asymmetric unit cell contains three p53 core domains and one DNA duplex. Although one p53 protomer is bound specifically to a

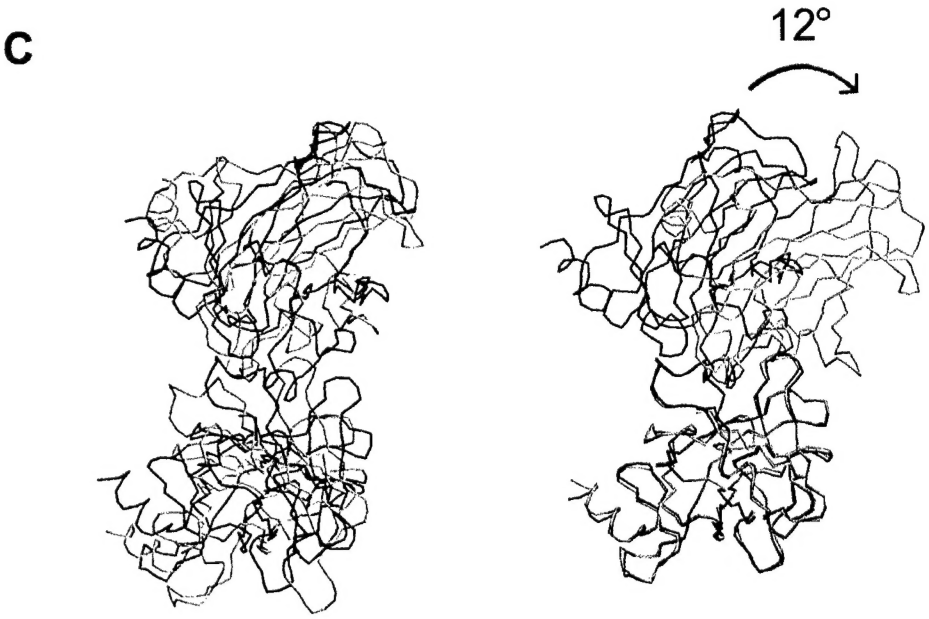

FIG. 4—*continued*

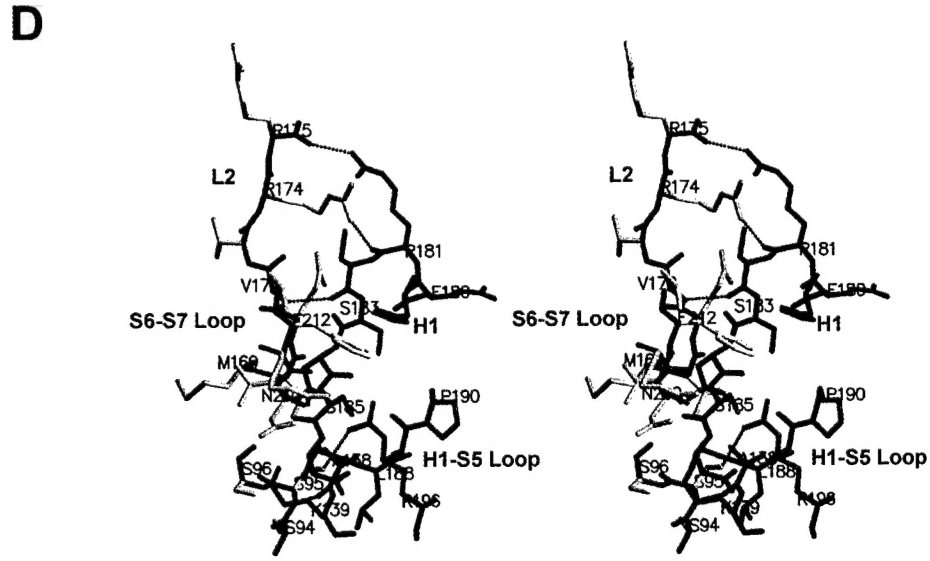

consensus pentameric DNA site, a second p53 protomer is bound nonspecifically at the junction of two DNA duplexes, and a third p53 protomer is not associated with DNA but is involved in dimer contacts with the DNA-binding p53 protomer in the asymmetric unit cell. Strikingly, these dimer contacts are very similar to the dimer contacts that are observed in the DNA-free mouse p53 core domain crystals reported here. Specifically, the same secondary structural elements are involved, the H1-S5 loop of one subunit and the S4-H1 (L2) and S6-S7 loops of the other subunit. Moreover, although the details of the contacts are different, many of the same residues are used to stabilize the dimer. Notably, Arg-174, Arg-181, and Glu-180 (analogous to Arg-171, Arg-178, and Glu-177 in the DNA-free dimer) play important roles in mediating H bonds within the dimer. Phe-212 and Pro-191 (analogous to Phe-209 and Pro-188 in the DNA-free dimer) also mediate Van der Waals interactions within the dimer (Fig. 4*D*).

In addition to the common interactions within the dimer interface of the DNA-free and DNA-containing p53 core domain crystals, there are several divergent interactions resulting in a somewhat different disposition of the two subunits of the dimer when the DNA-bound and DNA-free forms are compared. The overall root mean square deviation between the two p53 dimers is 5.5 Å (Fig. 4*C*). However, a superposition of one of the two subunits reveals that the other subunits of the corresponding dimers are related by a 12 ° rotation of one relative to the other. Taken together, the dimer contacts observed in two different p53 crystal lattices show striking similarity, although there appears to be some flexibility in the details of the interactions that stabilize the dimer.

Biological Implications of Dimer Contacts within the p53 Core Domain—In light of the similar p53 dimer contacts that are present within the crystal lattices of the mouse and human p53 core domain, we investigated the aggregation properties of the mouse p53 core domain in solution. To do this we carried out sedimentation equilibrium ultracentrifugation using two different protein concentrations and three different centrifugation speeds. Analysis of the data revealed a sedimentation profile that could be best fit by a monomer-dimer model fixing the molecular mass to the size of 22,695 Da with a K_d of 2.1 mM

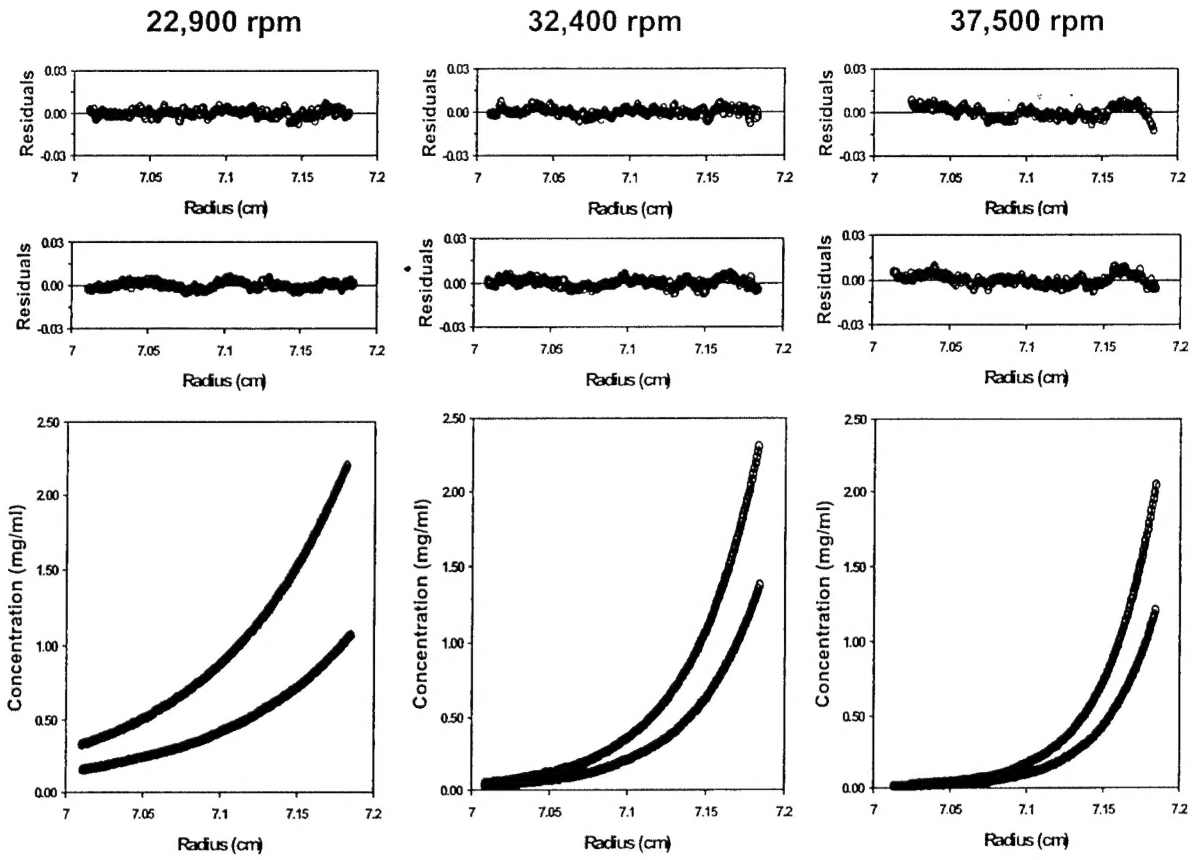

FIG. 5. **Equilibrium sedimentation ultracentrifugation of the mouse p53 core domain.** Two different initial protein concentrations (0.5 mg/ml (*lower curve*) and 1.5 mg/ml (*upper curve*)) were run at each of three different centrifugation speeds (as indicated in the *headings*). The *bottom panels* show concentration distribution plots along the filtered *curves* assuming a single species.

for low levels of dimer formation (Fig. 5). This model for slight oligerimerization, characterizing reversible monomer-dimer equilibrium, was significantly better than a single species model or models describing monomer-trimer or monomer-dimer-tetramer equilibrium. Taken together, the sedimentation equilibrium ultracentrifugation results clearly demonstrate that the isolated mouse p53 core domain is predominantly monomeric at physiological protein concentrations.

In light of these results, what can be the biological implications of the p53 dimer contacts that are observed in the crystals? *In vivo* p53 exists in a tetrameric form largely due to the presence of a highly conserved C-terminal tetramerization domain. Therefore the four *in vivo* p53 core domains are at high local concentrations and furthermore have an enhanced propensity to form specific interactions with each other. Given the tetrameric form of the p53 protein, the most likely interactions between the core domains would be either a dimer of dimers (as observed for the isolated tetramerization domain) or a symmetrical tetramer. For sequence-specific DNA binding, p53 has also been proposed to undergo a conformational change from a state with low affinity for DNA (T state) to a state with high affinity for DNA (R state) (6, 13). These different physiological states of p53 have been proposed based on the activities of antibodies that specifically react with and enhance one of the two states. Based on p53 DNA target sites that are two head to tail decamer repeats of 2-fold symmetric pentameric sites, the p53 conformation with high affinity for DNA is proposed to have the core domains aligned as two 2-fold symmetric dimers. Based on our crystallographic results, we propose that in the context of the p53 tetramer the core domain is arranged as a dimer of dimers and that the core domain dimer observed in our crystals represents a low affinity DNA state. This is consistent with the observation that the dimer in our crystals is

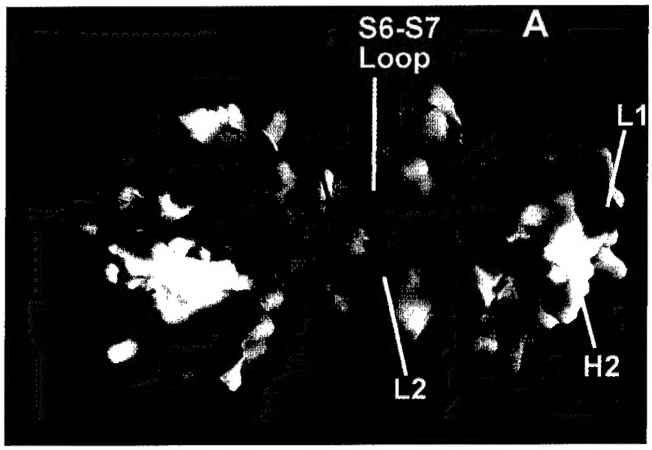

FIG. 6. **Electrostatic surface of the mouse p53 core domain dimer.** The electrostatic potential is calculated with the program GRASP (Nicholls *et al.*, 1991) and displayed as a color gradient from *red* (electronegative ≤ -10 kilotesla/charge) to *blue* (electropositive, ≥ 10 kilotesla/charge). *A* and *B* indicate subunits A and B of a noncrystallographic dimer of the unit cell.

configured in such a way that it is incompatible with simultaneous binding to duplex DNA. It is also consistent with the observation that a similar dimer is observed in the crystals of the human p53 core domain in the presence of DNA and in which only one of two subunits of the dimer make specific contacts to DNA. An electrostatic potential energy surface of the p53 core domain dimer in our crystals revealed a pronounced electropositive charge patch along one face of the dimer (Fig. 6). This surface may form a docking site for an acidic region of the p53 protein such as the N-terminal transactivation domain in the low affinity DNA binding state. Such

an interaction would also serve to mask the transactivation domain of p53 prior to high affinity DNA binding.

In conclusion, we have determined the crystal structure of the mouse p53 core domain and have compared it with the DNA-bound form of its human homologue. The comparison reveals that DNA binding by the core domain is accompanied by the reconfiguration of a loop region for major groove interactions with the DNA. Strikingly, we observe dimers of p53 core domains in our crystals in a configuration that is incompatible with simultaneous binding of both subunits to duplex DNA. A comparison with a similarly configured dimer in crystals of the human p53 core domain suggests that this dimer may represent a physiologically relevant low affinity DNA binding state of the p53 core domains in the context of the intact p53 tetramer. Further insights into the structural rearrangements mediated by p53 as a function of DNA binding will require structural analysis of the intact p53 tetramer in the presence and absence of DNA.

Acknowledgment—We thank Irina Kriksunov and Marian Szebenyi for help on beamline A1 at Cornell High Energy Synchrotron Source and R. Burnett for useful discussions.

REFERENCES

1. Prives, C., and Hall, P. (1999) *J. Pathol.* **187,** 112–126
2. Burns, T. F., and El-Deiry, W. S. (1999) *J. Cell. Physiol.* **181,** 231–239
3. Levine, A. J. (1997) *Cell* **88,** 323–331
4. Cho, Y., Gorina, S., Jeffrey, P. D., and Pavletich, N. P. (1994) *Science* **265,** 346–355
5. El-Deiry, W. S., Tokino, T., Velculescu, V. E., Levy, D. B., Parsons, R., Trent, J. M., Lin, D., Mercer, W. E., Kinzler, K. W., and Vogelstein, B. (1993) *Cell* **75,** 817–825
6. Halazonetis, T. D., and Kandil, A. N. (1993) *EMBO J.* **12,** 5057–5064
7. Friedman, P. N., Chen, X. B., Bargonetti, J., and Prives, C. (1993) *Proc. Natl. Acad. Sci. U. S. A.* **90,** 3319–3323
8. Stenger, J. E., Tegtmeyer, P., Mayr, G. A., Reed, M., Wang, Y., Wang, P., Hough, P. V. C., and Mastrangelo, I. A. (1994) *EMBO J.* **13,** 6011–6020
9. Pavletich, N. P., Chambers, K. A., and Pabo, C. O. (1993) *Genes Dev.* **7,** 2556–2564
10. Wang, Y., Reed, M., Wang, P., Stenger, J. E., Mayr, G., Anderson, M. E., Swhwedes, J. F., and Tegtmeyer, P. (1993) *Genes Dev.* **7,** 2575–2586
11. Tokino, T., Thiagalingam, S., Eldeiry, W. S., Waldman, T., Kinzler, K. W., and Vogelstein, B. (1994) *Hum. Mol. Genet.* **3,** 1537–1542
12. El-Deiry, W. S., Kern, S. E., Pietenpol, J. A., Kinzler, K. W., and Vogelstein, B. (1992) *Nat. Genet.* **1,** 45–49
13. Waterman, J. L. F., Shenk, J. L., and Halazonetis, T. D. (1995) *EMBO J.* **14,** 512–519
14. Clore, G. M., Ernst, J., Clubb, R., Omichinski, J. G., Kennedy, W. M., Sakaguchi, K., Appella, E., and Gronenborn, A. M. (1995) *Nat. Struct. Biol.* **2,** 253–254
15. Jeffrey, P. D., Gorina, S., and Pavletich, N. P. (1995) *Science* **267,** 1498–1502
16. Lee, W., Harvey, T. S., Yin, Y., Litchfield, D., and Arrowsmith, C. H. (1994) *Nat. Struct. Biol.* **1,** 877–890
17. Leslie, A. G. W. (1992) in *CCP4 and ESF-EACMB Newsletter on Protein Crystallography*, Darsbury Laboratory, Darsbury, U. K.
18. Navaza, J. (1994) *Acta Crystallogr. Sect. A* **50,** 157–163
19. Jones, T. A. (1978) *J. Appl. Crystallogr.* **11,** 268–272
20. Brunger, A. T., Adams, P. D., Clore, G. M., DeLano, W. L., Gros, P., Grosse-Kunstleve, R. W., Jiang, J. S., Kuszewski, J., Nilges, M., Pannu, N. S., Read, R. J., Rice, L. M., Simonson, T., and Warren, G. L. (1998) *Acta Crystallogr. Sect. D Biol. Crystallogr.* **54,** 905–921
21. Brunger, A. T., and Krukowski, A. (1990) *Acta Crystallogr. Sect. A* **46,** 585–593
22. Rice, L. M., and Brunger, A. T. (1994) *Proteins* **19,** 277–290
23. Jiang, J. S., and Brunger, A. T. (1994) *J. Mol. Biol.* **243,** 100–115
24. Yphantis, D. A. (1964) *Biochemistry* **3,** 297–317
25. Johnson, M. L., Correia, J. J., Yphantis, D. A., and Halvorson, H. R. (1981) *Biophys. J.* **36,** 575–588
26. Laue, T. M., Shah, B. D., Ridgeway, T. M., and Pelletier, S. L. (1992) in *Analytical Ultracentrifugation in Biochemistry and Polymer Science* (Harding, S. E., Rowe, A. J., and Horton, J. C., eds) pp. 90–125, The Royal Society of Chemistry, Cambridge, U. K.
27. Nicholls, A., Sharp, R. A., and Honig, B. (1991) *Proteins* **11,** 281–296